

Statistical Maps for EEG Dipolar Source Localization

Christian-G. Bénar*, *Student Member, IEEE*, Roger N. Gunn, Christophe Grova, Benoît Champagne, *Member, IEEE*, and Jean Gotman

Abstract—We present a method that estimates three-dimensional statistical maps for electroencephalogram (EEG) source localization. The maps assess the likelihood that a point in the brain contains a dipolar source, under the hypothesis of one, two or three activated sources. This is achieved by examining all combinations of one to three dipoles on a coarse grid and attributing to each combination a score based on an F statistic. The probability density function of the statistic under the null hypothesis is estimated nonparametrically, using bootstrap resampling. A theoretical F distribution is then fitted to the empirical distribution in order to allow correction for multiple comparisons.

The maps allow for the systematic exploration of the solution space for dipolar sources. They permit to test whether the data support a given solution. They do not rely on the assumption of uncorrelated source time courses. They can be compared to other statistical parametric maps such as those used in functional magnetic resonance imaging (fMRI).

Results are presented for both simulated and real data. The maps were compared with LORETA and MUSIC results. For the real data consisting of an average of epileptic spikes, we observed good agreement between the EEG statistical maps, intracranial EEG recordings, and fMRI activations.

Index Terms—Bootstrap resampling, dipole modeling, EEG/MEG source analysis, electroencephalography, inverse problems, model selection, source scanning, statistical map.

I. INTRODUCTION

THE electroencephalogram (EEG) is a recording of electrical potentials at a set of electrodes placed on the scalp. Though it is a measurement at the surface of the head, the EEG can still be used in an attempt to infer the location of the neural electrical sources within the brain that produce given EEG potentials, for example epileptic spikes or somatosensory evoked potentials. This localization problem is commonly referred to as the inverse problem of electroencephalography; a similar problem is found for the magnetoencephalogram (MEG). For a review of the electromagnetic inverse problem, see [1].

The inverse problem is ill-posed as there is an infinite number of source configurations that can produce the exact same potential at the surface of the head. However, if one assumes that the sources are made of current dipoles, with a small number of dipoles [2] and a sufficient number of electrodes [3], [4], then

Manuscript received January 13, 2004; revised June 27, 2004. This work was supported by the Canadian Institutes for Health Research (CIHR) under grant MOP 38079. C. G. Bénar holds a CIHR Doctoral Studentship. *Asterisk indicates corresponding author.*

*C.-G. Bénar is with the Montreal Neurological Institute, McGill University, Montreal, QC H3A 2B4, Canada (e-mail: christian.benar@mail.mcgill.ca).

R. N. Gunn, C. Grova, and J. Gotman are with the Montreal Neurological Institute, McGill University, Montreal, QC H3A 2B4, Canada.

B. Champagne is with the Department of Electrical Engineering, McGill University, Montreal, QC H3A 2B4, Canada.

Digital Object Identifier 10.1109/TBME.2004.841263

the solution is unique [5]. The dipolar model [6] is a reasonable approximation for focal sources [7] (for a review of dipolar methods, see [8]). Unfortunately, even with the dipolar assumption, different combinations of sources can produce very similar potential patterns. As a consequence, the inverse problem of EEG becomes even more ambiguous in the presence of background noise that can be higher than the difference between the potentials of such combinations.

Several groups have investigated the ambiguity of the electromagnetic inverse problem. For a given number of sources, the uncertainty in the source location parameters was quantified by defining confidence intervals. This has been done using the Cramer-Rao bound [9]–[11], simulated data [12] or implanted sources [13]. Determining the number of sources is a difficult topic though, and this additional ambiguity has also been a subject of much interest. For example, classical goodness of fit and model order selection criteria can help in selecting which model is better suited to the data [14], [15]. A widely used approach is based on principal component analysis (PCA) [16]. Indeed, for uncorrelated source time courses, the number of sources is given by the number of singular values significantly greater than zero. These nonzero singular values define a signal subspace that can be scanned using one dipole only; peaks in the scan indicate possible locations of the sources; this is the MUSIC method [17]. Drawbacks of the PCA decomposition are that it can be difficult to define the dimension of the signal subspace, and that PCA fails to find the number of sources when the time courses are fully correlated (even though a refinement of the MUSIC method has been proposed for handling fully correlated sources [18]). Another way to explore the brain volume is to use spatial filtering, or “beamforming” [19]. The efficiency of beamforming is also sensitive to the level of correlation of the sources, although it has been shown to be robust for a medium level of correlation [20].

A sensible way to reduce the ambiguity in the location parameters is to incorporate constraints originating from anatomical considerations, such as forcing sources to be distributed on the cortical surface and oriented perpendicular to it [21]. However, when using distributed sources, the very large number of sources results in an underdetermined problem. Regularization methods need to be introduced, such as a that of minimum energy [22] or of maximal smoothness [23]. Another type of constraint involves the use of data from other functional imaging modalities, such as functional magnetic resonance imaging (fMRI) [24], [25].

As the electromagnetic inverse problem is ambiguous, some authors have advocated an approach that avoids considering only a single “best” solution, but rather estimates a probability distribution of solutions [26], [27]. They used a Bayesian

framework that allows the incorporation of *a priori* knowledge in a formal way. In [27], the posterior distribution is sampled with the Markov Chain Monte Carlo (MCMC) technique; in [28] this approach is implemented within a maximum likelihood framework. The beamforming technique can be also be used in order to built statistical parametric maps [29].

In this paper, we investigate the ambiguity in both number and localization of dipolar sources, by exploring all the combinations of one to three dipolar sources on a coarse grid. This exhaustive search is made possible by limiting the resolution and the number of sources. We give to each combination of sources a score based on a statistical measure that reflects how well it describes the data. This is to be contrasted with the methods that first establish a best-fit solution and then estimate a confidence interval on the parameters of the solution [9]–[11]. We then build a three-dimensional (3-D) map assessing for each elementary volume (or voxel) the likelihood that it contains a source by summing the scores of all combinations containing this voxel.¹

The systematic exploration of the solution space is usually referred to as “dipole scanning.” The advantage of a scan with multiple sources is to permit the recovery of sources with perfect correlation, and also to avoid the potential local minima that exist in minimization-based approaches. The integration of the results when there is more than one source has not to our knowledge been reported. We propose a method for integrating at each point the results over all possible combinations, whereas the multiple-source scanning of [18] is searching for an optimum combination. The attribution of a score at each point of the head resembles the MUSIC scan [17]. However, we perform statistical measures that allow for the assessment of the significance of the scores, contrary to the MUSIC measure.

Our statistical approach is related to that of [27], but differs in several aspects. First, we use simple statistical tests in a frequentist framework. Second, it is an easier method to implement as it does not require MCMC computations. Third, we introduce in our scoring scheme a model order criterion that helps to reject additional sources that merely describe noise. Furthermore, we do not rely solely on a parametric description of the noise distribution that would make the statistical tests very dependent on the (difficult) estimation of the noise covariance matrix. Instead, we use empirical techniques in order to determine the distributions of our statistics.

In Section II, we introduce the statistical framework and concepts. We present in detail our method in Section III. In Section IV, we introduce the data used for validating the method. In Section V, we present the results of the validation with both simulation and real data, and of a comparison with the LORETA [23] and MUSIC [17] methods. The maps obtained for real data are compared to fMRI activations and intracranial EEG recordings belonging to the same patient.

II. STATISTICAL FRAMEWORK

A. The Linear Model

We assume that the EEG signal that we observe can be modeled by a set of s dipolar sources at locations $\theta_i = (x_i, y_i, z_i)$, $i \in \{1, \dots, s\}$. Each source is represented by a basis of three colocalized orthonormal dipoles describing any possible dipolar activity inside a given region [17], [30]. For each source, we define $\mathbf{x}(\theta_i)$ as the (n channels \times 3 dipoles) matrix whose columns are the potentials created by the corresponding three orthonormal dipoles.

The classical linear model for the EEG signal in the presence of noise is

$$\mathbf{Y} = \mathbf{X}(\Theta)\mathbf{B} + \mathbf{E} \quad (1)$$

where \mathbf{Y} is the spatiotemporal data matrix (n channels \times p time points); in order to enhance the signal-to-noise ratio (SNR), \mathbf{Y} is generally resulting from the average of k identical events. $\mathbf{X}(\Theta) = [\mathbf{x}(\theta_1), \dots, \mathbf{x}(\theta_s)]$ is the sensor array matrix (n channels \times $3s$ dipoles), $\Theta = [\theta_1, \dots, \theta_s]$ contains the dipole location parameters, \mathbf{B} contains the dipole waveforms ($3s$ dipoles \times p time points) and \mathbf{E} is the error matrix (n channels \times p time points). In the following sections, we will generally drop the reference to Θ to simplify the notations.

Each channel of EEG data is recorded with respect to a reference signal; this means that the rank of \mathbf{Y} is $\min\{n - 1, p\}$; this is also reflected in the degrees of freedom (DOFs) for the statistical tests in Section II-C.

The error matrix \mathbf{E} can be broken down into “pure EEG noise” \mathbf{E}_{eeg} , i.e., the error arising from background EEG activity superimposed on the signal, and “model error” $\mathbf{E}_{\text{model}}$, i.e., the part of the signal that has not been explained by the model [15]

$$\mathbf{E} = \mathbf{E}_{\text{eeg}} + \mathbf{E}_{\text{model}}. \quad (2)$$

Typically, the EEG error \mathbf{E}_{eeg} is assumed to be multivariate Gaussian. The model error $\mathbf{E}_{\text{model}}$ is the term we seek to minimize by selecting the correct number and location of sources. The time course \mathbf{B} of the dipoles can be further projected onto temporal basis functions [31]; this has the advantage of taking into account known temporal properties such as smoothness [32] and of reducing the number of parameters to estimate.

The classical statistical tests for the general linear model (1) require that the error \mathbf{E} be white and Gaussian [33]. The Gaussian assumption is reasonable for averaged EEG data with a high number of events k . However, the hypothesis of whiteness is strongly challenged as there is a high level of both temporal and spatial correlation in EEG data. An option is to preprocess the data to render the noise as uncorrelated as possible, using the covariance matrix of the noise Σ (“prewhitening” step, [34], [35]). Equivalently, one can incorporate Σ directly into the model and use the generalized least squares method [36], [37]. Using the information from Σ is important both during the fitting of the model, to avoid overfitting the noise, and during the inference step, to be able to

¹The term “likelihood” is used here in a general sense; this is not to be confused with the more strict statistical meaning, i.e., the probability of the observations given the parameters, seen as a function of the parameters.

model parametrically the noise properties (typically as a normal distribution). However, the estimation of Σ from data with a high level of spatio-temporal correlation is a difficult operation. Indeed, a full Σ describing all possible covariances has a dimension of $np \times np$ and has $np(np + 1)/2$ free elements. It is possible to reduce considerably the number of free elements in Σ by assuming that it is the Kronecker product of an $n \times n$ spatial covariance matrix Σ_S and a $p \times p$ temporal covariance matrix Σ_T [35]. Still, in order to estimate reliably the spatial covariance, one needs at least $n(n + 1)/2$ independent $n \times 1$ time points. This can be quite demanding, especially given the constraint of having a stationary EEG for the estimation procedure. An option is to perform more “robust” estimation by assuming a further constrained structure, such as a covariance decaying with distance [38].

B. Estimation of Parameters

We assume as in [35] that the prewhitening process can be separated into a spatial matrix \mathbf{W}_S and a temporal matrix \mathbf{W}_T . The prewhitened signal is then $\tilde{\mathbf{Y}} = \mathbf{W}_S \mathbf{Y} \mathbf{W}_T$. The spatial transformation must also be applied to the array matrix: $\tilde{\mathbf{X}} = \mathbf{W}_S \mathbf{X}$.

Under the assumption that $(\tilde{\mathbf{X}}^T \tilde{\mathbf{X}})$ is full rank, an estimate $\hat{\mathbf{B}}$ of the (temporally prewhitened) source amplitude parameters can then be computed by ordinary least squares [33]

$$\hat{\mathbf{B}} = (\tilde{\mathbf{X}}^T \tilde{\mathbf{X}})^{-1} \tilde{\mathbf{X}}^T \tilde{\mathbf{Y}}. \quad (3)$$

The matrix of residuals is formed by projecting the prewhitened data onto the subspace orthogonal to that spanned by the columns of $\tilde{\mathbf{X}}$

$$\mathbf{R} = \tilde{\mathbf{Y}} - \tilde{\mathbf{X}} \hat{\mathbf{B}} = (\mathbf{I} - \tilde{\mathbf{X}} (\tilde{\mathbf{X}}^T \tilde{\mathbf{X}})^{-1} \tilde{\mathbf{X}}^T) \tilde{\mathbf{Y}}. \quad (4)$$

C. Model Testing

1) *Goodness of Fit*: One may want to assess if the model accounts properly for the signal, i.e., if residuals are only noise. Typically, the residuals $\text{vec}(\mathbf{R})$ are hypothesized to be distributed with a multivariate normal distribution $\mathcal{N}(\mathbf{0}, \mathbf{I})$, with $\mathbf{0}$ $np \times 1$ vector of zeros and \mathbf{I} $np \times np$ identity matrix.

The residuals sum of squares, or “sum of squared errors,” is the square distance between the model and the data

$$\text{SSE} = \text{tr}(\mathbf{R}^T \mathbf{R}). \quad (5)$$

Under the hypothesis of normally distributed residuals, (5) has a χ^2 distribution with DOF $df(s) = (n - 1 - 3s)p$.

2) *Model Order*: Increasing the order of the model, i.e., the number of sources, is likely to result in a reduction of the sum of squared errors (5), as the residuals are formed by projecting the data onto a smaller subspace in (4). It is therefore important to test whether this reduction is significant, i.e., if the reduction is larger than that expected if the additional source was only explaining noise. For a given combination of s sources, and a reduced model with $(s - 1)$ sources, the null hypothesis $H_0^{(\text{order})}$ is that the portion of the sum of squares explained by the additional source has a χ^2 distribution. A simple test of model order uses the following statistic:

$$F = \frac{df(s)}{df(s-1) - df(s)} \frac{\text{SSE}^{s-1} - \text{SSE}^s}{\text{SSE}^s} \quad (6)$$

where SSE^s is the sum of squared errors for the fit with s sources and SSE^{s-1} is the sum of squared errors for the reduced model. Under the null hypothesis $H_0^{(\text{order})}$, (6) has an F distribution with DOF $(df(s-1) - df(s)) = 3p$ and $df(s) = (n - 1 - 3s)p$.

III. CONSTRUCTION OF STATISTICAL MAPS OF ACTIVATION

In order to construct a map for s sources, we consider all the combinations of s sources on a grid. For each combination, we compute an F test using spatially prewhitened data, that assesses if the data support the hypothesis of s sources versus $(s-1)$. We then compute a score at a given point of the grid by integrating the scores of all the combinations containing this point that pass a threshold of significance. The thresholds are computed using bootstrap resampling.

A. Prewhitening

We perform spatial prewhitening using an estimate of the spatial covariance matrix

$$\hat{\Sigma}_S = \mathbf{Z} \mathbf{Z}^T \quad (7)$$

where \mathbf{Z} is a (n channels $\times L$ time points) spatiotemporal matrix containing averaged background EEG. We assume that the averaged background noise was stationary across the matrix \mathbf{Z} . The size L of the background window is a compromise: it needs to be large in order to perform a correct estimation of the noise properties, but choosing too large a window increases the chances of incorporating spikes in the background or having a nonstationary window [39].

The matrix $\hat{\Sigma}_S$ is broken down based on a singular value decomposition

$$\hat{\Sigma}_S = \mathbf{U} \Lambda \mathbf{U}^T \quad (8)$$

with

$$\Lambda = \begin{pmatrix} \lambda_1 & & (0) \\ & \ddots & \\ (0) & & \lambda_n \end{pmatrix} \quad (9)$$

matrix of singular values and \mathbf{U} the matrix of eigenvectors. The spatial prewhitening filter is then defined as

$$\mathbf{W}_S = \begin{pmatrix} \frac{1}{\sqrt{\lambda_1}} & & (0) & 0 \\ & \ddots & & \vdots \\ (0) & & \frac{1}{\sqrt{\lambda_{n-1}}} & \vdots \\ 0 & \dots & \dots & 0 \end{pmatrix} \mathbf{U}^T. \quad (10)$$

We set the last diagonal element in (10) to zero as the rank of \mathbf{Z} , and thereby that of $\hat{\Sigma}_S$, is $(n - 1)$. Indeed, each channel of EEG data is always recorded versus the signal of the same reference electrode. We do not perform any temporal prewhitening, i.e., $\mathbf{W}_T = \mathbf{I}_p$.

B. Testing the Combinations

The statistical maps are constructed on a spatial grid of N points $P_j = (x_j, y_j, z_j)$, $j \in \{1, \dots, N\}$. In order to obtain a map for s sources, $s \in \{1, 2, 3\}$, we consider all combinations of s grid points with parameters Θ_k^s , $k \in \{1, \dots, C_N^s\}$, where $C_N^s = (N!)/(s!(N - s)!)$. For each combination, we create

an sensor array matrix $\mathbf{X}(\Theta_k^s)$ (cf. Section IV-A) and perform a least square fit with (3). For this combination, we compute the sum of squares errors $\text{SSE}(\Theta_k^s)$ with (5) and the F statistic $F(\Theta_k^s)$ with (6). We define Θ_{\min}^s as the parameters that give the lowest sum of squared errors across all combinations of s sources, i.e., the best fit

$$\Theta_{\min}^s = \arg \min_{\Theta_k^s} (\text{SSE}(\Theta_k^s)). \quad (11)$$

For a given combination of s sources with location Θ_k^s , the F value (6) is defined versus the combination with one less source that gave the lowest sum of squared errors: $\text{SSE}^{s-1} = \text{SSE}(\Theta_{\min}^{s-1})$. For the one-dipole scan, we use the data total sum of squares as SSE^{s-1} . We are thereby testing that the combination with s sources is an improvement on the best solution with $(s-1)$ sources.

C. Computing the Scores

The score for the combination Θ_k^s is defined as

$$\sigma_k = \begin{cases} F(\Theta_k^s) & \text{if } F(\Theta_k^s) \geq \text{thr}_F(s), \\ 0 & \text{otherwise.} \end{cases} \quad k \in 1, \dots, C_N^s \quad (12)$$

with $\text{thr}_F(s)$ the significance threshold at the order s (cf. Section III-D).

At each point P_j of the grid, $j \in \{1, \dots, N\}$, we integrate the scores of all the combinations containing this point and normalize by the number of combinations

$$\text{map}(P_j, s) = \frac{\sum_{\{k | P_j \in \Theta_k^s\}} \sigma_k}{C_{N-1}^{s-1}} \quad (13)$$

which reflects the likelihood that this grid point contains a source under the hypothesis of s sources.

D. Computation of Thresholds

In order to compute the thresholds for the statistical tests, we estimate empirically the distribution of the F statistic (6) under the null hypothesis (i.e., the additional source is only explaining noise). To do so, we construct a set of 5000 realizations \mathbf{E}_b^* , $b \in \{1, \dots, 5000\}$ of realistic averaged EEG noise \mathbf{E}_{eeg} .

Each realization \mathbf{E}_b^* of the noise is obtained by drawing at random with replacement sections of 20 consecutive points (100 ms) from the averaged background \mathbf{Z} (i.e., one could obtain in one realization several copies of the same section). Enough sections are joined together in order to obtain a matrix \mathbf{E}_b^* with the same number of columns as the original signal of length p . This is the ‘‘moving block bootstrap’’ for serially correlated data, as described in [40]. Our assumptions are that the averaged background is stationary and sufficiently long to represent well the variability of the underlying stochastic process, and that the length of the sections is sufficient to preserve the temporal structure of the process. This implies that each realization \mathbf{E}_b^* has the same statistical properties as the original averaged EEG background.

We fit the model to each realization as in (3)

$$\hat{\mathbf{B}}_b^{s,*} = \left[\tilde{\mathbf{X}}(\Theta_{\min}^s)^T \tilde{\mathbf{X}}(\Theta_{\min}^s) \right]^{-1} \tilde{\mathbf{X}}(\Theta_{\min}^s)^T \tilde{\mathbf{E}}_b^* \quad (14)$$

where $\tilde{\mathbf{E}}_b^* = \Sigma_S \mathbf{E}_b^*$ is the prewhitened noise, and $\Theta = \Theta_{\min}^s$, $s \in \{1, 2, 3\}$ are the parameters corresponding to the combination of sources that produced the lowest sum of squared errors when fitted to the data (11). We then compute the statistics $\text{SSE}_b^*(s)$ using (5) and $F_b^*(s)$ using (6), with $\text{SSE}^{s-1} = \text{SSE}_b^*(s-1)$. For $s = 1$, we use the sum of squares of $\tilde{\mathbf{E}}_b^*$ as SSE^{s-1} . At each s , we compute the empirical distributions (histograms) of $F_b^*(s)$, $b \in \{1, \dots, 5000\}$.

In a second step, the estimated thresholds need to be corrected for multiple comparison. However, the empirical distributions of $F_b^*(s)$ typically have an insufficient sampling of the tails for this procedure. Therefore we fit to each empirical distribution a theoretical F distribution by varying the corresponding DOFs; we use a nonlinear minimization method (simplex algorithm). We then compute the thresholds $\text{thr}_F(s)$ corresponding to the $p = 0.05$ percentile corrected with the Bonferroni method, i.e., $p = 0.05/C_N^s$.

IV. EVALUATION OF THE METHOD

We analyzed three data sets in order to evaluate the capacities of our method for localizing sources and assessing dipolar models. The first set was an idealized configuration consisting of two simulated dipoles located on the grid used for scanning, with potentials corrupted by Gaussian noise correlated in space but not in time. The second data set was a more realistic situation, where we simulated extended patches of cortex, with real EEG noise added. The third set was a real average of epileptic spikes, obtained on a patient for whom we had functional MRI and intracerebral EEG results.

For each data set, we computed on a 10-mm grid the statistical maps for one to three dipoles, as well as a MUSIC scan and a LORETA current density reconstruction. The MUSIC and LORETA methods are the versions implemented in the Curry software (Neuroscan Labs). For MUSIC, we included in the signal subspace the eigenvectors corresponding to the singular values above the level of the noise.

A. Model Computations

We computed all possible components of the array matrix \mathbf{X} with the Curry 4.5 software (Neuroscan, El Paso, TX). The computations used a boundary element method (BEM) realistic head model based on the subject’s own MRI scan, with BEM surfaces corresponding to the brain (7-mm mesh), skull (10-mm mesh) and skin (12-mm mesh) [41]. Conductivities were set to $0.33 \text{ S}\cdot\text{m}^{-1}$, $0.0083 \text{ S}\cdot\text{m}^{-1}$, and $0.33 \text{ S}\cdot\text{m}^{-1}$, respectively (ratio of skull to brain of 1/40). We created a uniform square grid inside the brain volume with 10-mm spacing; points corresponding to deep brain structures were not included. To enhance computation speed for the scan for $s = 3$ sources, a low-resolution 15-mm spacing grid was also created. For each point of the grids, we computed the potentials generated by three unit orthogonal dipoles. The average of all channels was subtracted from the potential at each channel.

B. Idealized Simulation

We computed the potentials of two simulated radial dipoles located symmetrically in the left and right central regions. We

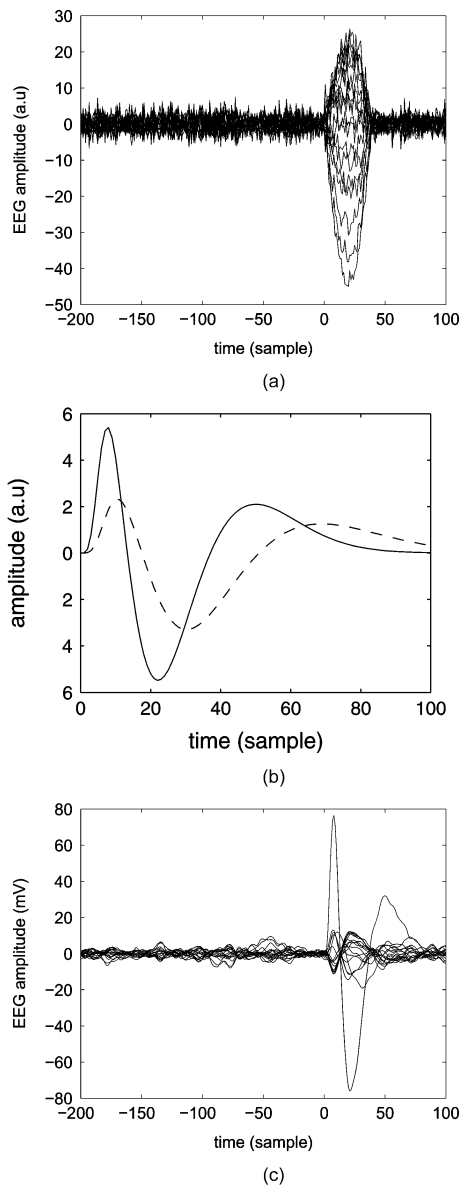


Fig. 1. Simulated data: temporal characteristics. The sampling frequency is 200 Hz. (a) EEG data for the idealized simulation (two central radial dipoles on the grid); only the 10–20 channels and 200 samples of background are shown. The SNR is 10 (ratio of sum of squares across all channels and time points). (b) Source time courses for the realistic simulation (one temporal patch and one frontal patch). Solid line: temporal source, dashed line: frontal source. The first peak of the frontal source is delayed by 3 samples (15 ms). The time courses were scaled to have the same energy. (c) Data for the realistic simulation; only the 10–20 channels and 200 samples of background are shown. The SNR is 50.

used the head model built for the patient data (cf. Section IV-A). The time course of both dipoles was a half-period of a sine wave, lasting 40 samples; the two dipoles were perfectly synchronous. The background noise (1000 samples) was generated by assigning to each unit dipole on the 10-mm grid a pseudo-random amplitude following a Gaussian distribution, similarly to [42]. This ensured spatial correlation and temporal whiteness of the noise. The potentials created by the sources were scaled in order to obtain a signal to noise ratio of 10 (ratio of total sum of squares across time and channels). Fig. 1 shows the simulated data.

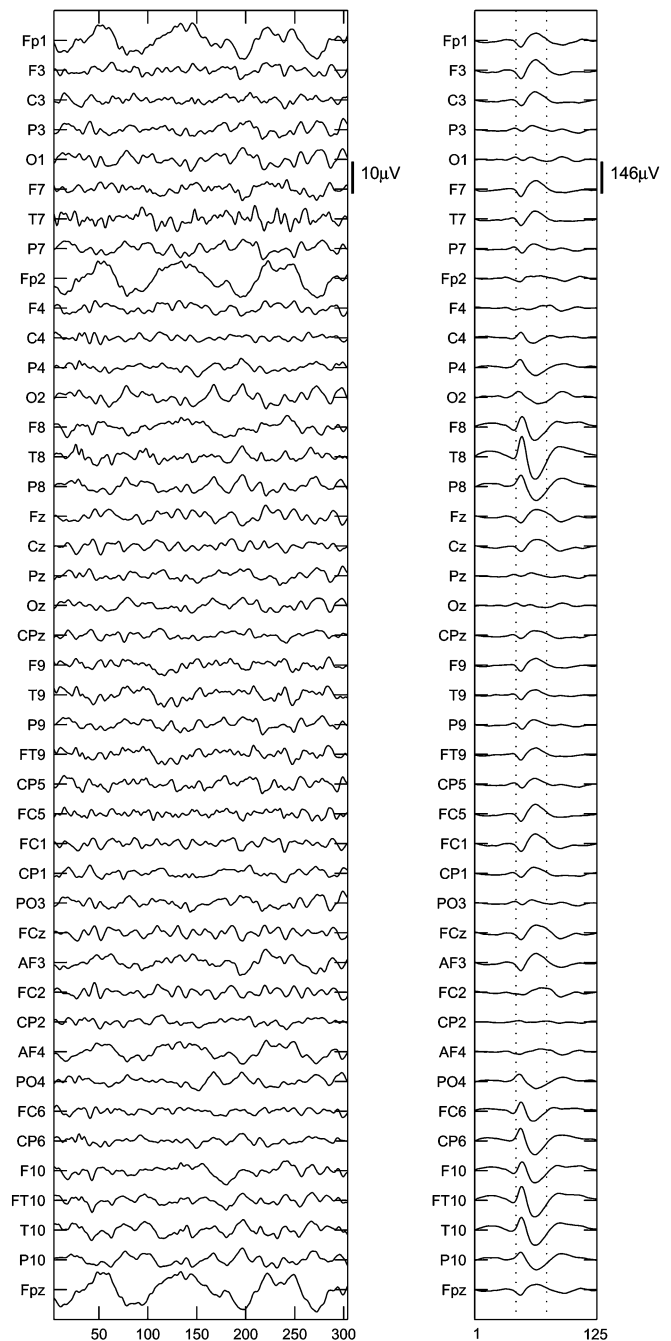


Fig. 2. Two sections of 43-channel EEG, created by averaging 23 epileptic spikes (patient data). Left panel: a section of averaged background. Right panel: the average spike, with maximum amplitude in the right temporal region (channels T8, T10, FT10); the dotted lines mark the section selected for computing the maps. Time is in samples (sampling frequency: 200 Hz). The SNR is 296.5. Note that the amplitude scale is different between panels.

C. Realistic Simulation

We created an $n \times p$ ($n = 43, p = 34$) spatiotemporal data matrix by adding the potentials generated by two simulated sources to real EEG background noise sampled at $F_s = 200$ Hz. The first source was placed in the lateral part of the temporal lobe. The second source was in the frontal region. The time course of the first source was obtained by adding three consecutive

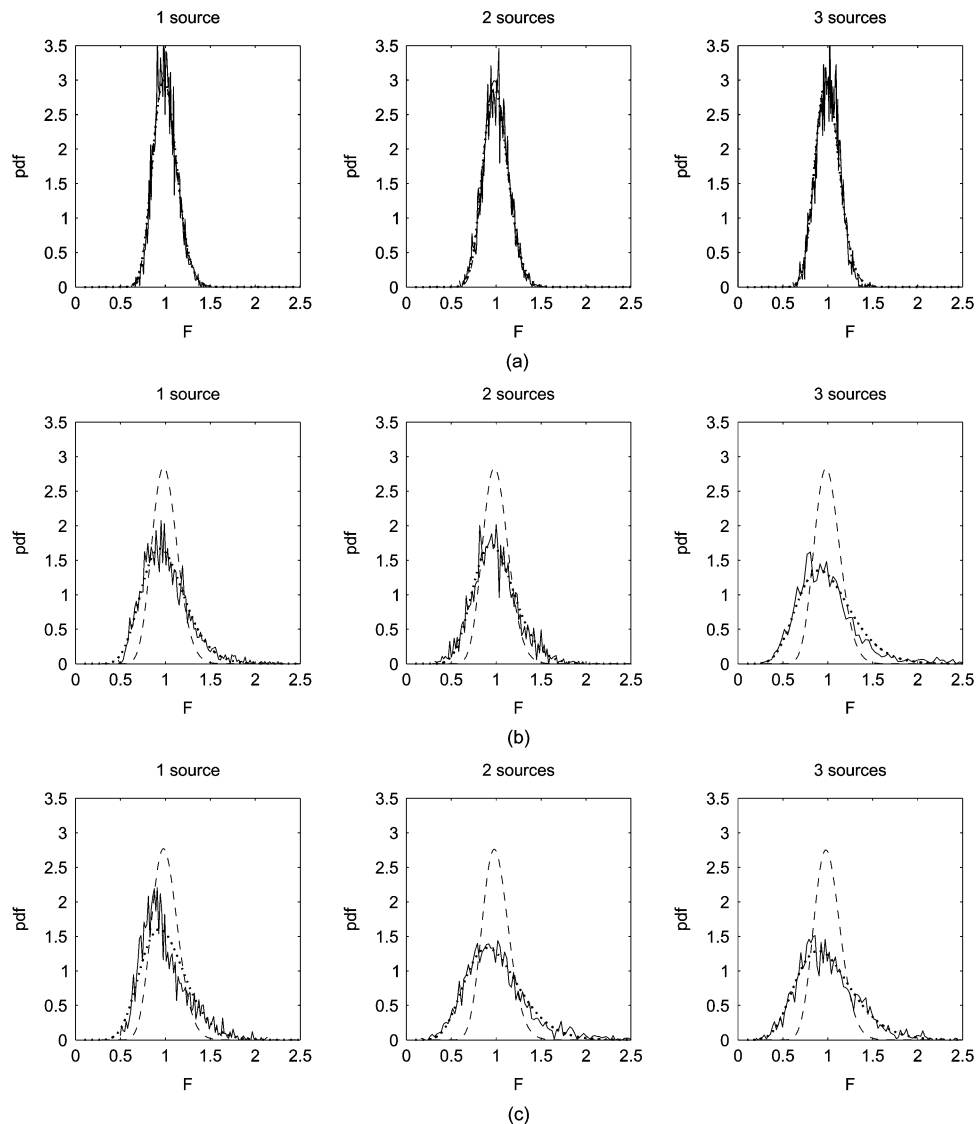


Fig. 3. Empirical distributions of the F statistics for one to three sources. On each graph, the theoretical distributions for white Gaussian noise is shown in dashed line. The fitted F distribution are in dotted lines. For the realistic simulation and the patient data, the empirical distribution are broader than the theoretical distributions, due to the remaining correlations in the EEG data. (a) Idealized simulation. (b) Realistic simulation. (c) Patient data.

gamma functions peaking at 40 ms, 110 ms and 250 ms, respectively. The parameters of the gamma functions were obtained by fitting the real average spike presented in the next section. The time course of the frontal source was obtained by stretching that of the first source in order to have the first peak delayed by 15 ms, which is a reasonable value for neuronal propagation [cf. Fig. 1(b)].

We simulated each realistic source as a patch of cortex. We used a 2-mm mesh of the cortical surface, obtained from the MRI of the patient presented in next section, and placed a dipole at each vertex in the direction normal to the mesh. A patch was defined as a set of dipoles within a sphere of radius 1.3 cm (i.e., of section $\pi \cdot 1.3^2 \simeq 5.3 \text{ cm}^2$). The background noise was obtained by adding 20 sections of real EEG with no spike obtained from the patient described in next section. The sum of the source potentials was scaled so as to have a signal to noise ratio of 100 (ratio of total sum of squares across time and channels). Fig. 1(c) shows a butterfly plot of the data.

D. Patient Data

The EEG data consisted of a 43-channel spatio-temporal matrix resulting from the average of $k = 23$ epileptic spikes sampled at a frequency $F_s = 200$ Hz, from a patient with focal epilepsy. The spikes were chosen to be as similar as possible, in terms of spatial distribution and temporal waveform. The spikes were aligned by cross-correlation before averaging. The EEG was filtered with a band-pass filter set from 1.6 Hz to 35 Hz. The averaging and filtering was performed with the BESA software (Megis, Munich, Germany). The data was “referenced to the average”, i.e., the average of all channels was subtracted from the data at each time point. We defined a signal window of $p = 34$ samples (170 ms), i.e., the portion of interest of the averaged EEG spike, and a background noise window of $L = 1000$ samples (5 s), i.e., an average of $k = 23$ EEG sections preceding each spike and not containing spikes. The first point of the background window was set to 2000 samples (10 s)

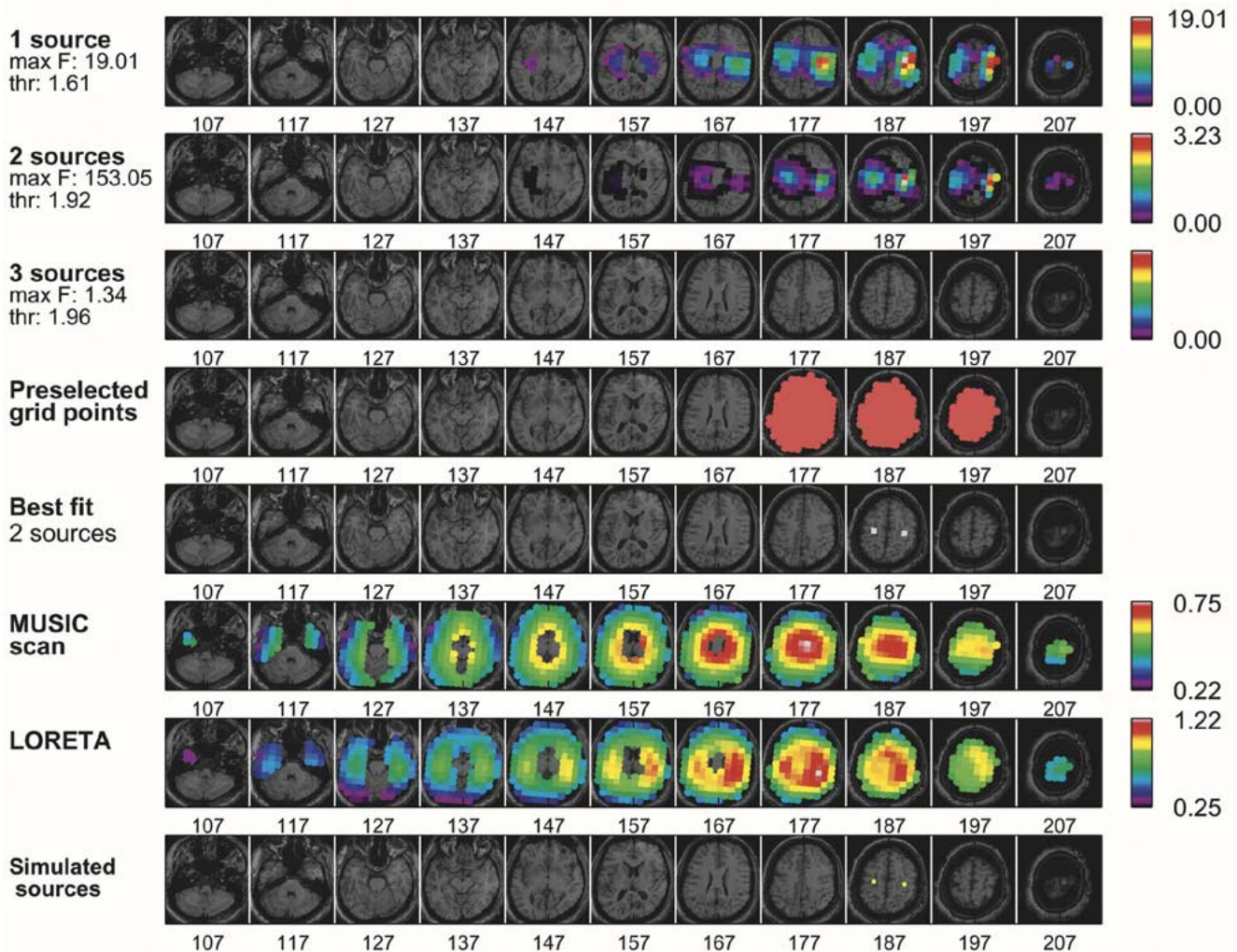


Fig. 4. Statistical maps $\text{Map}(P_j, s)$ for one, two and three sources for the idealized simulation. The F threshold and the F score corresponding to the combination with the best fit are displayed on the left of each map. In the fourth row, the (manually) preselected grid points are shown. In the last row, the actual locations of the two simulated dipoles are shown. Abscissae: elevation in millimeters (z axis). Voxels with a value of zero are not shown; those in black correspond to very low nonzero values. The locations of the dipoles are detected as local maxima in the maps for two sources ($z = 187$). No combination of three dipoles was significant. The MUSIC 1-dipole scan was unable to separate the sources. LORETA correctly identified two peaks, but at $z = 177$.

before the spike, as the background immediately preceding the spike was contaminated with spikes. The signal window was chosen to encompass the spike itself and the slow-wave that follows (Fig. 2). The signal to noise ratio was 296.5 (ratio of total sum of squares across time and channels).

For this patient, we also had intracranial EEG recordings, anatomical and functional MRI data. The intracranial recordings were performed during presurgical evaluation. The fMRI protocol consisted of recording 19 EEG channels (10/20 system) inside the MR scanner (details in [43]). The timing of the EEG spikes was used for the statistical analysis of the fMRI images. We then recorded the EEG outside the scanner, adding 24 electrodes (10/10 system) for a total of 43 electrodes. It is the recording outside the scanner that we used for computing the data matrix \mathbf{Y} . As the 10/20 electrodes were visible on the anatomical scan recorded during the fMRI protocol, we could mark them onto the realistic head model. The remaining 10/10 electrodes were placed manually on a 3-D rendering of the head surface.

E. Computation Time

The computation time for each scan is a function of C_N^s . In order to reduce the computation time for the three-source scan, we used a multiresolution approach to restrict the search to a subset of the grid. We first computed the scores on a 15-mm grid, and retained the points in the 10-mm grid whose nearest neighbor in the 15-mm grid had a nonzero value.

The total computing time for the scans on the 15-mm grid (311 points) was 1 h 04 min. For the idealized simulation (cf. Section IV-B), the number of selected points in the 10-mm grid was 251 out of 836 (30%). The total computing time for the 10-mm scans, with the three-source scan on the restricted grid, was 1 h 37 min. For the realistic simulation (cf. Section IV-C), 68 points (8.1%) were preselected. The computation time for the scans on the 10-mm grid was 4 min 59 s. For the patient data, the number of selected points was 82 out of 836 (9.8%). The total computing time for the 10-mm scans was 4 min 37 s.

We used a Pentium M laptop with a processor speed of 1.4 GHz and 512 Mb of RAM. The algorithm was implemented with the Matlab software (Mathworks, Natick, MA).

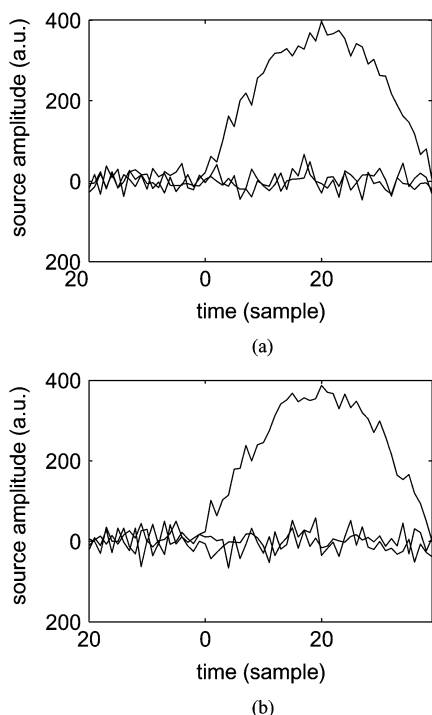


Fig. 5. Reconstructed time course for the idealized simulation, for sources placed at the local maxima of the map for two sources. For each source, a basis of three orthogonal dipoles is used. The data displayed is reconstructed using a singular value decomposition of the source time course (this is equivalent to having one dipole of the basis oriented along the direction of higher variance). The time courses of the main component correspond very well to the simulated waveforms for both sources (half sine wave of period 40 samples). (a) First local maximum. (b) Second local maximum.

V. RESULTS

A. Empirical Distributions of F

Fig. 3 displays the empirical distributions of $F_b^*(s)$ (6) for one to three sources, for both simulated and patient data, along with the theoretical F distributions (corresponding to the assumption of white gaussian residuals) and the fitted F distributions (cf. Section III-D).

For the idealized simulation, the empirical distributions are very close to the theoretical distribution [Fig. 5(a)], showing that the spatial prewhitening was efficient in removing the spatial correlations. For both realistic simulation and the patient data [Fig. 3(b) and (c)], the empirical distributions are broader than the theoretical F distribution. This is likely to reflect the fact that there is still some correlation left in the data—thereby decreasing the effective DOFs. Indeed, we did not perform temporal prewhitening in order to preserve the signal [35] and the spatial covariance was estimated on a limited number of time points in order to ensure stationarity and avoid contamination by spikes.

The fitted distributions generally represent well the empirical distributions. However, for the real background EEG, there is a tendency for the empirical distribution to have a thicker tail than the fitted distribution, which is more prominent for three sources [Fig. 3(b) and (c)]. This may suggest that in our examples the real EEG background is not perfectly Gaussian.

B. Maps for Idealized Simulation

The maps resulting from processing the idealized simulated data (cf. Section IV-B) are shown in Fig. 4. The grid points with nonzero values permit to assess the extent of the regions where the hypothesis of a dipolar source is supported by the data.

The one-source map, which is simply the significant F scores, displays the grid points where one dipole explains a significant portion of the data. There is a large number of points with a high score in both left and right regions, with a right predominance that likely reflects the fact that this source contributed more to the signal (as the two sources are not perfectly symmetrical).

For the two-source map, which represents the integration of the scores of all combinations of two dipoles, the maps present two local peaks at the correct dipole locations ($z = 187$). The maps are more focused around the true dipole locations, which could be because the criterion (significance of two dipoles versus one) is stricter than for the one-source map (significance of one dipole versus none). Another effect is that the two-source map is created by averaging over a large number of combinations, which favors points that are present in a large number of combinations.

The maximum F score for two sources is 153, which shows that the data strongly support the hypothesis of two dipolar sources versus one dipolar source. In contrast, the map for three sources is blank, which shows that the method correctly rejected the hypothesis of three dipolar sources.

The MUSIC scan (signal subspace of dimension one) finds one peak in the middle of the simulated dipoles, as expected because of the perfect correlation of the sources. The LORETA method correctly identifies two peaks, but at a lower z -value ($z = 177$). This lower value of z could be a consequence of the smoothness constraint or of the partial prewhitening (only the diagonal of the covariance matrix was used).

We present in Fig. 5 the time courses reconstructed by considering a dipolar source at each local maximum of the two-source map. The time courses correspond very well to the simulated waveform.

C. Maps for Realistic Simulation

The maps resulting from processing the realistic simulated data (cf. Section IV-C) are shown in Fig. 6. In the maps for one and two sources, a large number of points have a nonzero value, including the areas corresponding to the sources but also the region lying between the two simulated sources. The points that stand out are all in the left temporal region. This reflects the fact that the temporal source contributes much more to the data than the frontal source (the SNRs for the temporal and frontal sources considered separately are 46.7 and 3.3, respectively).

The map for three sources shows that there are significant combinations of three dipolar sources that can explain the data, although only two sources have been simulated. This can be explained by the fact that the simulated sources are not single dipoles lying perfectly on the grid as in the idealized simulation, and therefore require more than two dipoles to explain fully the signal. Nevertheless, the points with higher values are in the correct regions. The match is very good for the temporal source, as the global maximum lies around the location of the center of

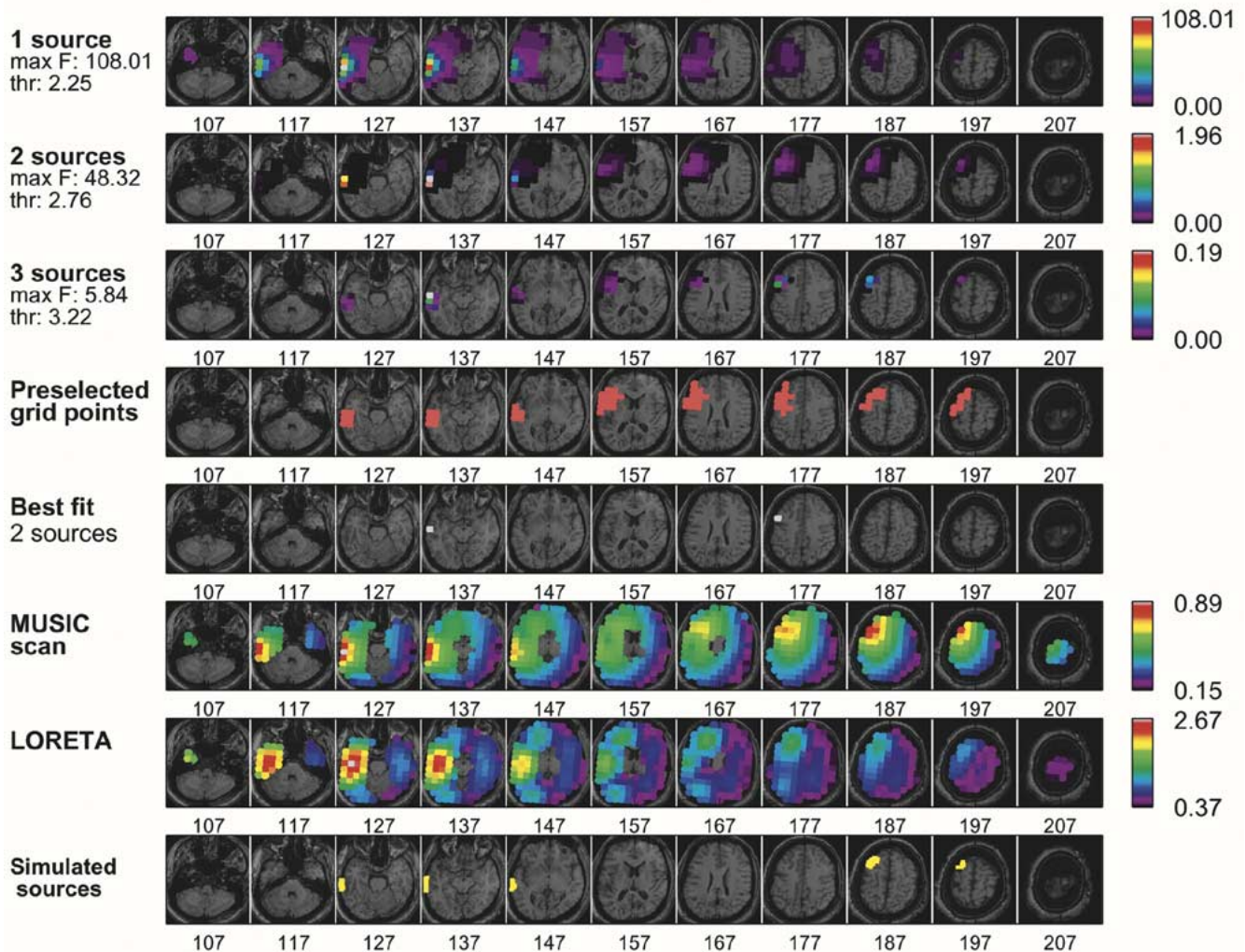


Fig. 6. Statistical maps $\text{Map}(P_j, s)$ for one, two and three sources for the realistic simulation. The F threshold and the F score corresponding to the combination with the best fit are displayed on the left of each map. In the last row, the actual locations of the two simulated patches are shown. Abscissae: elevation in millimeters (z axis). Voxels with a value of zero are not shown; those in black correspond to very low nonzero values. The locations of the patches correspond to grid points with high values in the maps three sources ($z = 137$ and $z = 177$ – 187). As the number of sources increase, the maps become more focused toward the center of gravity of the patches. Both MUSIC (signal subspace of dimension two) and LORETA identify two regions of activation. For both, the global maxima corresponding to the temporal source ($z = 127$) are displaced to a lower z value with respect to the center of gravity of the patch.

gravity of the patch. The points are displaced to a lower z -value for the frontal source. The maximum F score is much higher for the two-source maps than for the three-source map (48.3 versus 5.8), showing that the impact of going from one source to two sources is higher than when going from two sources to three sources.

Both MUSIC (signal subspace of dimension two) and LORETA identify two regions of activation. For both, the global maxima corresponding to the temporal source ($z = 127$) are displaced to a lower z value with respect to the center of gravity of the patch. Only MUSIC was able to detect the frontal source at the exact z location ($z = 187$), whereas both LORETA and our method found this frontal source displaced to a lower z -value ($z = 167$ and $z = 177$ respectively). The MUSIC scan is the method that gives the best contrast for the frontal source.

We present in Fig. 7 the time courses reconstructed by considering a dipolar source at each local maximum of the two-sources map. For the temporal source, the time course corresponds very

well to the simulated waveform. The waveform of the frontal source is more difficult to retrieve because of the lower SNR of this source. However, it is still possible to see that the source is activated with a delay with respect to the temporal source.

D. Maps for Patient Data

Fig. 8 presents the maps for the patient data, as well as the intracranial EEG (SEEG) electrodes and the functional MRI t-stat map. The threshold of $t = 3$ for the fMRI map implies that five contiguous points need to be above the threshold in order to have a cluster significant at $p = 0.05$ (corrected, [44]).

In the map for one source, the right temporal region ($z = 114$) presents the highest values. The activated region extends all the way up to the right superior parietal region. In the maps for two and three sources, the global maximum is still temporal at $z = 124$ and additional local maxima appears in the inferior frontal region ($z = 144$ and $z = 154$ for the two- and three-sources, respectively) and in the right parietal region ($z = 164$ for both).

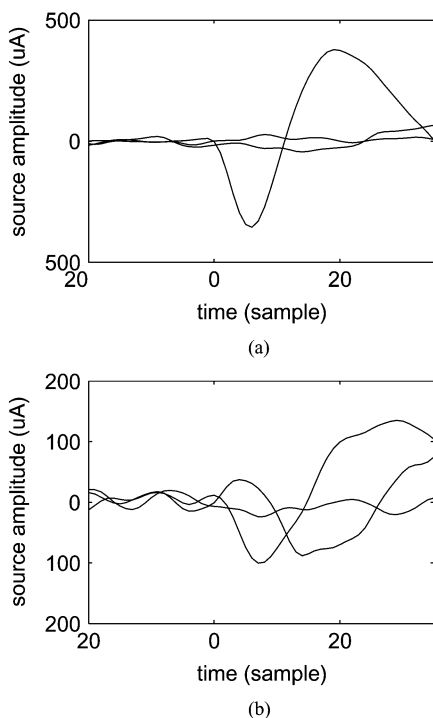


Fig. 7. Reconstructed time course for the realistic simulation, for sources placed at the local maxima of the map for two sources. For each source, a basis of three orthogonal dipoles is used. The data displayed is reconstructed using a singular value decomposition of the source time course (this is equivalent to having one dipole of the basis oriented along the direction of higher variance). For the temporal source (top), which has the higher SNR, the waveform is well reconstructed in the main component. For the frontal source (bottom), the waveform is more difficult to visualize because of the lower SNR of this source. The first peak of the main component permits nevertheless to see that this source is activated with a delay. (a) First local maximum. (b) Second local maximum.

The MUSIC scan (subspace dimension of three) finds local maxima only in the temporal region; however the three regions found with the statistical maps present high values. The LORETA method finds local maxima in the temporal ($z = 124$) and parietal regions ($z = 164$), but none in the lower frontal region (even though there are still relatively high values in this region).

There is no SEEG electrode at the level of the temporal global maximum at $z = 124$, but it is located just below activated SEEG electrodes at $z = 134$. The inferior frontal local maximum in the three-source map ($z = 154$) is at the level of an activated SEEG electrodes; this local maximum corresponds to one dipole of the best fitting combination.

The activated SEEG electrodes at $z = 144$ also correspond to a high value in the three-source map. The SEEG electrode closer to the parietal local maximum is active ($z = 164$). This local maximum does not correspond to any dipole of the best fitting combination. Moreover, it is located at the level of the fMRI cluster ($z = 154 - 164$).

Given the fact that the spatial resolutions of the different techniques (EEG dipole localization, fMRI at 1.5 T and SEEG) are of the order of 1 cm [13], [45], our cross-modality results are compatible with one another. The peak in the EEG map that is closest to the fMRI activation is that with the lowest score, and the other peaks do not correspond to any fMRI activation. In

particular, this is the case for the main EEG peak in the inferior temporal region, possibly because of fMRI signal loss in this region due to a magnetic susceptibility effect. This suggests that one should be cautious when considering the possibility of a one-to-one correspondence between EEG and fMRI results, as pointed out in [46].

VI. CONCLUSION

We have presented a method for building statistical maps for EEG source localization. These maps assess for each point in the brain the likelihood that it contains a source by giving it a score based on a statistical test. They allow for the exploration of the solution space in a systematic way. This permits to assess the range of plausible solutions, but can also be useful in order to avoid the local minima that plague the minimization-based approaches. Contrary to a PCA decomposition, there is no need to assume that source time courses are uncorrelated. The maps also permit a comparison of the results obtained under the hypothesis of one, two or three dipolar sources. They are 3-D, contrary to a classical dipole solution and can be compared to other statistical parametric maps, such as those used in functional MRI. Indeed, a region that is not a local maximum in the EEG and the fMRI maps but still leads to a significant score in both maps would increase the confidence that this region is active.

We use a test of model order at each level that assesses if the data support the addition of another source. The use of a threshold permits to restrict the result to the combinations where all the sources contribute to the model. Summing up the scores of the combinations at each point enables to visualize the results in a condensed manner. It also enhances the points contained in several plausible combinations, which we assume are more likely to contain a true source. Indeed, less weight should be given to spurious detections that appear only in a few combinations, whereas true sources should be part of a large number of combinations.

The information on the number of sources that is supported by the data is very important in EEG dipole modeling. Our results for the realistic simulation point to a limitation of a dipolar scan in that sense. Indeed, as real sources are not lying on a grid and are not point sources, but rather extended patches of cortex, the F test of model order results in a number of dipoles larger than the number of activated patches. We expect this limitation to have also a strong impact on the sum of squares (5), as a large number of sources will be needed to bring the residuals below the level of the noise.

The localization results we obtained in both simulated and real data are very encouraging. In the simulated data, the maps presented peaks consistent with the locations of the sources. In the real data, the peaks in the scan corresponded well with both depth EEG and fMRI results. Quantitative evaluation on real data remains difficult, though, due to the limited spatial sampling of depth EEG. Further simulations will be required with different combinations of sources and noise levels, as well as more tests on patient data.

We have compared our localization results to those obtained with two well-known methods, namely a MUSIC scan and LORETA, which also produce 3-D maps of activity. On the

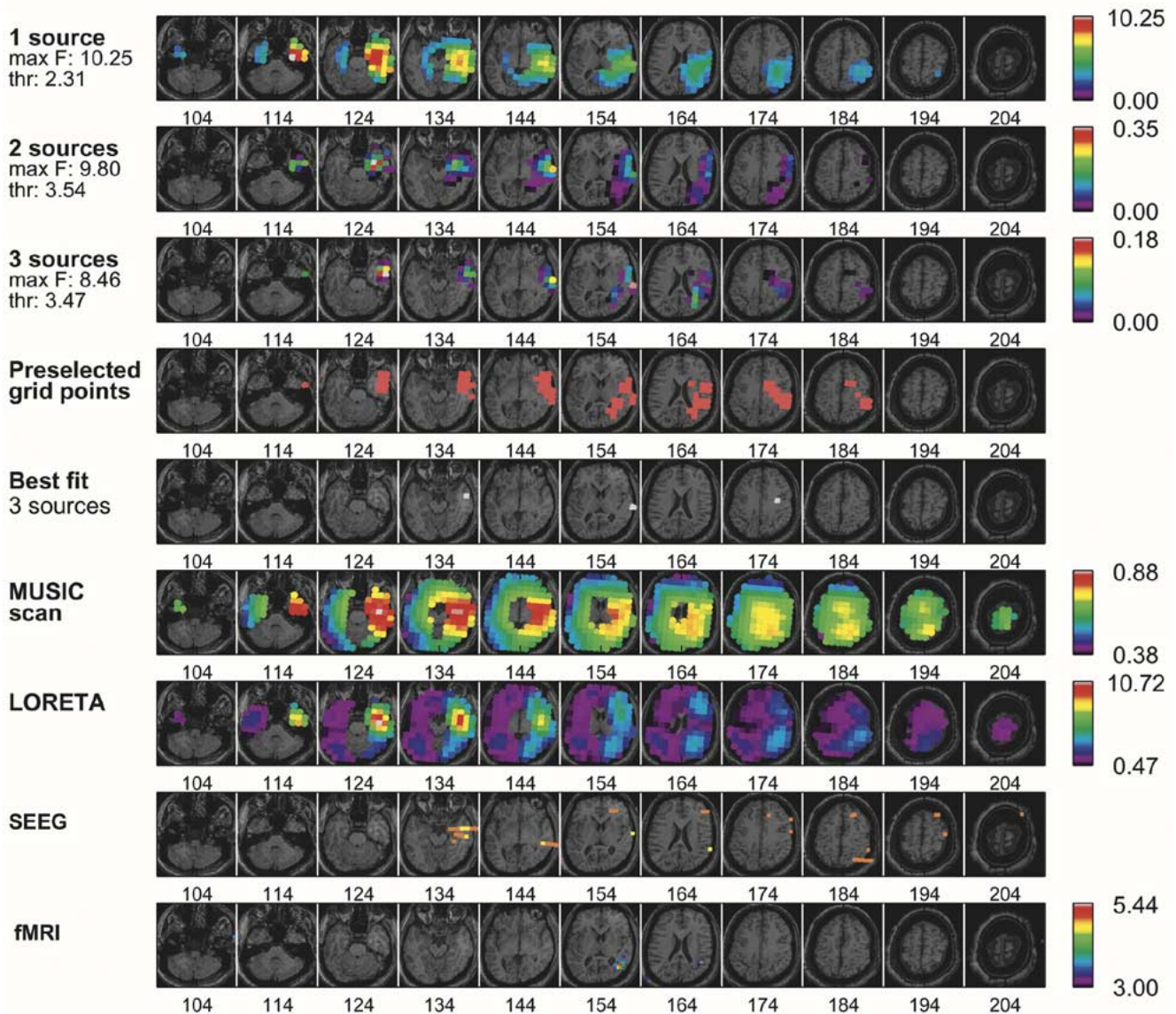


Fig. 8. Statistical maps $\text{Map}(P_j, s)$ for one, two and three sources for the patient data, compared with MUSIC and LORETA results, depth EEG recordings (SEEG, electrodes with spiking activity in yellow, other electrodes in orange) and functional MRI (t-stat map). The F value corresponding to the combination with the best fit and the corresponding threshold are displayed on the left of each map. In the fourth row, the grid points that have been preselected are shown. Abscissae: elevation in millimeters (z axis). For the EEG maps, the value at each point is the mean score across all combinations containing the point. For the fMRI map, the values are t-statistics. In the three-source map, the global maximum at $z = 124$ in the anterior temporal region is located below activated intracerebral electrodes at $z = 134$. The local maximum at $z = 154$ in the inferior frontal region corresponds well to an activated subdural electrode at $z = 154$. The local maximum in the parietal region at $z = 164$ is just above the fMRI main cluster of activation ($z = 154$). The MUSIC scan finds local maxima only in the temporal region. The LORETA method finds local maxima in the temporal and parietal region, but none in the lower frontal region.

data presented, our method compares well with MUSIC and LORETA in terms of detection capacities. Only our method was able to detect the fully correlated sources at the correct location. The variation of MUSIC for correlated sources proposed in [18] would probably have been able to detect these sources too; however we also display with our method the 3-D extent of plausible dipolar solutions. Our statistical approach could be compared to the noise-normalized implementations of the distributed sources methods [47], [48], which could be more suited for extended sources.

Generally speaking, all these methods should not be seen as antagonist, but as asking different questions with respect to the data. MUSIC and LORETA aim at finding the best solution in a given sense, the sources most correlated to the signal sub-

space for MUSIC and the spatially smoothest current density for LORETA. In our method, we aim at assessing whether a given combination of sources is supported by the data by using a statistical threshold. In addition, we combine all significant solutions to create a map of the likelihood of having a dipolar source at a given point.

We have used an empirical method for the computation of thresholds. This permits to take into account the fact that noise is strongly correlated, both spatially and temporally, and to adapt the tests accordingly. The other option would have been to rely solely on prewhitening of the data, which has two drawbacks: the robust estimation of the covariance matrix with highly correlated data is difficult, and temporal prewhitening can reduce the signal [35].

The models fitted in order to estimate the empirical distributions were based on the best solutions at level s and $(s - 1)$, mainly for computational reasons. The thresholds we obtain are expected to be conservative, as we use the lowest SSE at level s , i.e., that giving the highest F value. Also, the information on the significance of the best combination at level s with respect to the best at level $(s - 1)$ is valuable in the context of model-order selection. A refinement of the method could be to estimate the distributions by including different sources combinations in the bootstrap method.

When estimating the distributions under H_0 using bootstrap resampling, we chose to fit realizations of noise only (cf. (14)) and not to include signal. An option would have been to include in the bootstrap realizations the potentials generated by the best $(s - 1)$ sources. We do not expect this to have a high impact though. Indeed, by fitting the best combinations of $(s - 1)$ and s sources, most of the signal in the data generated by $(s - 1)$ sources should be removed, and any remaining signal should be at the level of the noise.

We have corrected our statistics for the multiple comparison problem. We have used a simple Bonferroni correction, which is likely to be conservative because of the dependence between the tests on different combinations. An empirical approach that would control the false positive rate by performing a large amount of scans on background noise (as in [49]) would be very computationally demanding, especially for the three-source scan. An alternative could be to define "resolution elements", i.e., sets of grid points for which the tests are highly correlated, as was done in fMRI [50]. However, we have not found in our simulated data that the Bonferroni correction was particularly conservative. This is possibly because the conservatism of the Bonferroni threshold is compensated by the fact that sources are not ideal dipoles, which leads to elevated F tests.

We have used a multiresolution approach, similar to [51]. This allowed us to obtain maps for three sources with a resolution of 10 mm, a reasonable performance in the context of spike localization for presurgical evaluation. Nevertheless, further restrictions on the scanned volume could allow for a finer resolution or a higher number of sources if this is deemed necessary.

ACKNOWLEDGMENT

C.-G. B. would like to thank Dr. K. Worsley, Dr. S. Baillet, and Dr. S. Kukreja for fruitful discussions, Dr. Y. Aghakhani for his help in reviewing the EEG data and Dr. A. Bagshaw for proofreading the manuscript.

REFERENCES

- [1] S. Baillet, J. Riera, G. Marin, J. Mangin, J. Aubert, and L. Garnero, "Evaluation of inverse methods and head models for EEG source localization using a human skull phantom," *Phys. Med. Biol.*, vol. 46, pp. 77–96, 2001.
- [2] M. Wax and I. Ziskind, "On unique localization of multiple sources by passive sensor arrays," *IEEE Trans. Acoust., Speech, Signal Process.*, vol. 37, no. 7, pp. 996–1000, Jul. 1989.
- [3] R. Srinivasan, P. L. Nunez, D. M. Tucker, R. B. Silberstein, and P. J. Cadusch, "Spatial sampling and filtering of EEG with spline laplacians to estimate cortical potentials," *Brain Topogr.*, vol. 8, no. 4, pp. 355–366, 1996.
- [4] C. Bénar and J. Gotman, "Non-uniform spatial sampling in EEG source analysis," in *Proc. 23rd Int. Conf. IEEE-EMBS*, vol. 1, Oct. 2001, pp. 903–905.
- [5] A. El Badia and T. Ha-Duong, "An inverse source problem in potential analysis," *Inverse Prob.*, vol. 16, pp. 651–663, 2000.

- [6] M. Brazier, "A study of the electric fields at the surface of the head," *Electroencephalogr. Clin. Neurophysiol.*, vol. 2, pp. 38–52, 1949.
- [7] J. de Munck, B. van Dijk, and H. Spekreijse, "Mathematical dipoles are adequate to describe realistic generators of human brain activity," *IEEE Trans. Biomed. Eng.*, vol. 35, no. 11, pp. 960–966, Nov. 1998.
- [8] B. N. Cuffin, "EEG dipole source localization," *IEEE Eng. Med. Biol. Mag.*, vol. 17, no. 5, pp. 118–122, Sep./Oct. 1998.
- [9] J. Mosher, M. Spencer, R. Leahy, and P. Lewis, "Error bounds for EEG and MEG dipole source localization," *Electroencephalogr. Clin. Neurophysiol.*, vol. 86, no. 5, pp. 303–321, 1993.
- [10] B. Radich and K. Buckley, "EEG dipole localization bounds and MAP algorithms for head models with parameter uncertainties," *IEEE Trans. Biomed. Eng.*, vol. 42, no. 3, pp. 233–241, Mar. 1995.
- [11] C. Muravchik and A. Nehorai, "EEG/MEG error bounds for a static dipole source with a realistic head model," *IEEE Signal Process. Mag.*, vol. 49, no. 3, pp. 470–484, Mar. 2001.
- [12] K. Kobayashi, H. Yoshinaga, M. Oka, Y. Ohtsuka, and J. Gotman, "A simulation study of the error in dipole source localization for EEG spikes with a realistic head model," *Clin. Neurophysiol.*, vol. 114, no. 6, pp. 1069–1078, 2003.
- [13] B. N. Cuffin, D. L. Schomer, J. R. Ives, and H. Blume, "Experimental tests of EEG source localization accuracy in realistically shaped head models," *Clin. Neurophysiol.*, vol. 112, no. 12, pp. 2288–2292, Dec. 2001.
- [14] S. Supek and C. J. Aine, "Simulation studies of multiple dipole neuromagnetic source localization: Model order and limits of source resolution," *IEEE Trans. Biomed. Eng.*, vol. 40, no. 6, pp. 529–540, Jun. 1993.
- [15] L. J. Waldorp, H. M. Huizenga, R. P. Grasman, K. B. Bocker, J. C. de Munck, and P. C. Molenaar, "Model selection in electromagnetic source analysis with an application to VEFs," *IEEE Trans. Biomed. Eng.*, vol. 49, no. 10, pp. 1121–1129, Oct. 2002.
- [16] I. Jolliffe, *Principal Component Analysis*. New York: Springer-Verlag, 1986.
- [17] J. Mosher, P. Lewis, and R. M. Leahy, "Multiple dipole modeling and localization from spatio-temporal MEG data," *IEEE Trans. Biomed. Eng.*, vol. 39, no. 6, pp. 541–557, Jun. 1992.
- [18] ———, "Recursive MUSIC: A framework for EEG and MEG source localization," *IEEE Trans. Biomed. Eng.*, vol. 45, no. 11, pp. 1342–1354, Nov. 1998.
- [19] K. Sekihara, S. Nagarajan, D. Poeppel, A. Marantz, and Y. Miyashita, "Reconstructing spatio-temporal activities of neural sources using an MEG vector beamformer technique," *IEEE Trans. Biomed. Eng.*, vol. 48, no. 7, pp. 760–771, Jul. 2001.
- [20] K. Sekihara, S. Nagarajan, D. Poeppel, and A. Marantz, "Performance of an MEG adaptive-beamformer technique in the presence of correlated neural activities: Effects on signal intensity and time-course estimates," *IEEE Trans. Biomed. Eng.*, pt. 2, vol. 49, no. 12, pp. 1534–46, Dec. 2002.
- [21] A. Dale and M. Sereno, "Improved localization of cortical activity by combining EEG and MEG with MRI cortical surface reconstruction: A linear approach," *J. Cogn. Neurosci.*, vol. 5, pp. 162–176, 1993.
- [22] M. Hämläinen and R. Ilmoniemi, "Interpreting magnetic fields of the brain: Minimum norm estimates," *Med. Biol. Eng. Comput.*, vol. 32, no. 1, pp. 35–42, 1994.
- [23] R. Pascual-Marqui, C. Michel, and D. Lehmann, "Low resolution electromagnetic tomography: A new method for localizing electrical activity in the brain," *Int. J. Psychophys.*, vol. 18, pp. 49–65, 1994.
- [24] A. Liu, J. Belliveau, and A. Dale, "Spatiotemporal imaging of human brain activity using functional MRI constrained magnetoencephalography data: Monte Carlo simulations," *Proc. Nat. Acad. Sci.*, vol. 95, no. 15, pp. 8945–8950, 1998.
- [25] N. Trujillo-Barreto, E. Martinez-Montes, L. Melie-Garcia, and P. Valdes-Sosa. (2001) A symmetrical bayesian model for fMRI and EEG/MEG neuroimage fusion. *Int. J. Bioelectromagn.* [Online], vol. (1). Available: <http://ee.tut.fi/rigi/ijbem/volume3/number1/valdesosa/index.htm>
- [26] C. Clarke, "Probabilistic methods in a biomagnetic inverse problem," *Inverse Prob.*, vol. 5, no. 6, pp. 999–1012, 1989.
- [27] D. Schmidt, J. George, and C. Wood, "Bayesian inference applied to the electromagnetic inverse problem," *Hum. Brain Mapp.*, vol. 7, no. 3, pp. 195–212, 1999.
- [28] W. E. Kincses, C. Braun, S. Kaiser, W. Grodd, H. Ackermann, and K. Mathiak, "Reconstruction of extended cortical sources for EEG and MEG based on a Monte-Carlo-Markov-chain estimator," *Hum. Brain Mapp.*, vol. 18, no. 2, pp. 100–110, 2003.
- [29] G. R. Barnes and A. Hillebrand, "Statistical flattening of MEG beamformer images," *Human Brain Mapping*, vol. 18, no. 1, pp. 1–12, 2003.
- [30] M. Scherg and D. von Cramon, "Evoked dipole source potentials of the human auditory cortex," *Electroencephalogr. Clin. Neurophysiol.*, vol. 65, no. 5, pp. 344–360, 1986.

- [31] A. Dogandžić and A. Nehorai, "EEG dipole source localization," *IEEE Trans. Signal Process.*, vol. 48, no. 1, pp. 13–25, Jan. 2000.
- [32] S. Baillet and L. Garnero, "A bayesian approach to introducing anatomic-functional priors in the EEG/MEG inverse problem," *IEEE Trans. Biomed. Eng.*, vol. 44, no. 5, pp. 374–385, May 1997.
- [33] M. S. Srivastava, *Methods of Multivariate Statistics*. New York: Wiley, 2002.
- [34] R. Beucker and H. A. Schlitt, "A study of the electric fields at the surface of the head," *Brain Topogr.*, vol. 10, pp. 168–169, 1997.
- [35] J. C. de Munck, H. M. Huizenga, L. J. Waldorp, and R. M. Heethaar, "Estimating stationary dipoles from MEG/EEG data contaminated with spatially and temporally correlated background noise," *IEEE Trans. Signal Process.*, vol. 50, no. 7, pp. 1554–1564, Jul. 2000.
- [36] K. Sekihara, D. Poeppel, A. Marantz, H. Koizumi, and Y. Miyashita, "MEG spatio-temporal analysis using a covariance matrix calculated from nonaveraged multiple-epoch data," *IEEE Trans. Biomed. Eng.*, vol. 46, no. 5, pp. 515–521, May 1999.
- [37] B. Lutkenhoner, "Dipole source localization by means of maximum likelihood estimation I. Theory and simulations," *Electroencephalogr. Clin. Neurophysiol.*, vol. 106, no. 4, pp. 314–321, 1998.
- [38] H. Huizenga, J. de Munck, L. Waldorp, and R. Grasman, "Spatiotemporal EEG/MEG source analysis based on a parametric noise covariance model," *IEEE Trans. Biomed. Eng.*, vol. 49, no. 6, pp. 533–539, Jun. 2002.
- [39] B. A. Cohen and A. J. Sances, "Stationarity of the human electroencephalogram," *Med. Biol. Eng. Comput.*, vol. 15, no. 5, pp. 513–518, 1977.
- [40] B. Efron and R. Tibshirani, *An Introduction to Bootstrap*. New York: Chapman & Hall, 1993.
- [41] M. Hämmäläinen and J. Sarvas, "Realistic conductivity geometry model of the human head for interpretation of neuromagnetic data," *IEEE Trans. Biomed. Eng.*, vol. 36, no. 2, pp. 165–171, Feb. 1989.
- [42] J. de Munck, P. Vijn, and F. L. da Silva, "A random dipole model for spontaneous brain activity," *IEEE Trans. Biomed. Eng.*, vol. 39, no. 8, pp. 791–804, Aug. 1992.
- [43] C. Bénar, Y. Aghakhani, Y. Wang, A. Izenberg, A. Al-Asmi, F. Dubeau, and J. Gotman, "Quality of EEG in simultaneous EEG-fMRI for epilepsy," *Clin. Neurophysiol.*, vol. 114, no. 3, pp. 569–580, 2003.
- [44] J. Cao, "The size of the connected components of excursion sets of χ^2 , t, and F fields," *Adv. Appl. Prob.*, vol. 31, pp. 577–593, 1999.
- [45] R. Turner, "How much cortex can a vein drain? Downstream dilution of activation-related cerebral blood oxygenation changes," *Neuroimage*, vol. 16, no. 4, pp. 1062–1067, 2002.
- [46] P. Nunez and R. Silberstein, "On the relationship of synaptic activity to macroscopic measurements: Does co-registration of EEG with fMRI make sense?," *Brain Topogr.*, vol. 13, no. 2, pp. 79–96, 2000.
- [47] A. Dale, A. Liu, B. Fischl, R. Buckner, J. Belliveau, J. Lewine, and E. Halgren, "Dynamic statistical parametric mapping: Combining fMRI and MEG for high-resolution imaging of cortical activity," *Neuron*, vol. 26, pp. 55–67, 2000.
- [48] R. Pascual-Marqui, "Standardized low resolution brain electromagnetic tomography (sLORETA): Technical details," *Methods Find Exp. Clin. Pharmacol.*, vol. 24, no. Suppl. D, pp. 5–12, 2002.
- [49] D. Pantazis, T. Nichols, S. Baillet, and R. M. Leahy, "Spatiotemporal localization of significant activation in MEG using permutation tests," in *Proc. Conf. Information Processing in Medical Imaging*, Jul. 2003.
- [50] K. Worsley, S. Marrett, P. Neelin, A. Vandal, K. Friston, and A. Evans, "A unified statistical approach for determining significant signals in images of cerebral activation," *Hum. Brain Mapp.*, vol. 4, pp. 58–73, 1996.
- [51] L. Gavit, S. Baillet, J. F. Mangin, J. Pescatore, and L. Garnero, "A multiresolution framework for MEG/EEG source imaging," *IEEE Trans. Biomed. Eng.*, vol. 48, no. 10, pp. 1080–1087, Oct. 2001.



Christian-G. Bénar (S'04) was born in Dijon, France, in 1971. In 1994, he received the engineering degree from Ecole Supérieure d'Electricité (Supélec), Paris and Metz, France, with a specialization in digital signal and image processing. He is currently working towards the Ph.D. degree in the department of biomedical engineering, McGill University, Montreal.

From 1994 to 1995, during his military service, he worked at the Institut de Médecine Navale in Toulon, France, as a member of the scientific contingent. From 1995 to 1997, he was a Software Developer at Stellate Systems, Montreal, QC, Canada. He joined the Montreal Neurological Institute in 1998. His research interests include statistical signal processing, source localization of epileptic spikes and simultaneous recordings of EEG and functional MRI.



Roger N. Gunn received the B.Sc. degree in applied mathematics in 1992 and the Ph.D. degree in engineering in 1996 from the University of Warwick, Warwick, U.K.

After completing the Ph.D. at the MRC Cyclotron Unit, Hammersmith Hospital, London, U.K., he continued working there as a Non-Clinical Scientist until March 2001. He then moved to the McConnell Brain Imaging Center, Montreal Neurological Institute, McGill University, Montreal, Canada, where he took up the position of Assistant Professor of Neurology and Neurosurgery. In 2002, he also became Assistant Professor of Biomedical Engineering. His research interests include neuroimaging, positron emission tomography, tracer kinetics, mathematical modeling, parametric imaging, ligand receptor interactions, and partial volume correction.



Christophe Grova was born in Créhange, France, in 1974. In 1998, he received both the engineering degree and the master's degree in biomedical engineering from the University of Technology of Compiègne, Compiègne, France, with a specialization in image and signal processing. In 1998, he joined the IDM laboratory (UPRES 3192, University of Rennes, France), where he received the Ph.D. degree in "Validation of SPECT/MRI registration methods in the context of epilepsy."

Since January 2003, he has been working with the team of Professor Jean Gotman at the Montreal Neurological Institute, Montreal, QC, Canada, as a Postdoctoral Fellow. His research interests are statistical signal processing, localization of epileptic spikes using distributed sources modeling, and validation of signal and image processing methods in the clinical context of epilepsy.



Benoît Champagne (S'87–M'89) was born in Joliette QC, Canada, in 1961. He received the B.Eng. degree in engineering physics from the Ecole Polytechnique of Montreal, QC, Canada, in 1983, the M.Sc. degree in physics from the University of Montreal in 1985, and the Ph.D. degree in electrical engineering from the University of Toronto, Toronto, ON, Canada, in 1990.

From 1990 to 1999, he was an Assistant and then Associate Professor at INRS-Télécommunications, Université du Québec, Montreal, where he remains appointed as a Visiting Professor. In September 1999, he joined McGill University, Montreal, as an Associate Professor within the Department of Electrical and Computer Engineering; he is currently acting as Associate Chairman of Graduate Studies. His research interests lie in the area of statistical signal processing, including signal/parameter estimation, sensor array processing, adaptive filtering, and their applications.



Jean Gotman received the engineering degree from Ecole Supérieure d'Electricité, Paris, France, in 1969, the M.S. degree in engineering from Dartmouth College, Hanover, NH, in 1971, and the Ph.D. degree in neurological sciences from McGill University, Montreal, QC, Canada, in 1976.

He is currently working at the Montreal Neurological Institute and Hospital and is a Professor in the Departments of Neurology and Biomedical Engineering of McGill University. He is also the founder and President of Stellate, a company making medical equipment for the analysis of brain signals. His research interests center on signal processing and pattern recognition of the EEG, particularly in the field of epilepsy and of long-term monitoring in the intensive care unit.